Griffiths phase on hierarchical modular networks with small-world edges

Shanshan Li

Phys. Rev. E **95**, 032306 — Published 6 March 2017

DOI: 10.1103/PhysRevE.95.032306

Griffiths Phase on Hierarchical Modular Networks with Small-world Edges

Shanshan Li
Department of Physics, Emory University, Atlanta, GA 30322; USA

The Griffiths phase has been proposed to induce a stretched critical regime that facilitates self-organizing of brain networks for optimal function. This phase stems from the intrinsic structural heterogeneity of brain networks, i.e. the hierarchical modular structure. In this work, the Griffiths phase is studied in modified hierarchical networks with small-world connections based on the 3-regular Hanoi network. Through extensive simulations, the hierarchical level-dependent inter-module wiring probabilities are identified to determine the emergence of the Griffiths phase. Numerical results and the complementary spectral analysis on the relevant networks can be helpful for a deeper understanding of the essential structural characteristics of finite dimensional networks to support the Griffiths phase.

PACS numbers: 05.70.Ln, 89.75.Hc, 89.75.Fb

I. INTRODUCTION

The well-known criticality hypothesis suggests biological systems operate at the borderline between the sustained active and inactive state. It has been observed in various processes such as gene expression [1], cell growth [2] and neuronal avalanches [3]. In different contexts, the critical point enables optimal transmission and storage of information [4, 5], maximal sensitivity to stimuli [6], optimal computational capabilities [7]. Empirical studies on brain networks [8–10], however, exhibit a stretched critical region. The Griffiths phase (GP), characterized by generic power-laws over a broad region in the parameter space, provides an alternative mechanism for critical behavior in brain networks without fine tuning [11, 12]. It is confirmed numerically and analytically that the structural heterogeneity induces the Griffiths phase that eventually enhances the self-organization mechanism of brain networks.

Brain networks have been found to be organized into modules across hierarchies [13–15]. Modules in each hierarchy are grouped into larger modules, forming a fractal-like structure. Previous work models brain networks with finite dimensional hierarchical modular networks (HMNs) [11, 12], and successfully confirms the existence of the Griffiths phase using dynamical models, such as the Susceptible-Infected-Susceptible (SIS) model and the Contact Process (CP). The essential characteristics of previous network models is the hierarchical level-dependent inter-module wiring probabilities. It is conjectured that plain modular networks are not able to support the Griffiths phase, and disorder in different scales significantly influences properties of critical behaviors [11]. In this work, the idea of a Griffith phase is extended to other hierarchical structures encountered in previous studies of dynamical processes on complex networks.

Certain hierarchical networks, with a self-similar structure and small-world connections, have shown to exhibit novel dynamics [16–21]. In this work, the hierarchical models are designed based on one such example with a finite topological dimension, the 3-regular Hanoi network [16, 18, 22, 23]. To tune the modular feature that is present in brain networks, a single node of the original network is modified into a fully connected clique with a varying size. By introducing different classes of inter-module connections, the essential heterogeneous connectivity pattern is explored to induce the Griffiths phase on finite dimensional networks. It turns out that the hierarchical level-dependent inter-module wiring probabilities plays an important role affecting the property of the phase transition at criticality.

As a complement to the computational approach, the spectral analysis on the adjacency matrix and the Laplacian matrix of networks is conducted. A localized principle eigenvector of the network adjacency matrix indicates the network heterogeneity, which has been used to quantify the localization of activity on networks above the critical propagation rate in the dynamical model [24]. This concept has been applied to analytically explain the emergence of rare regions and the Griffiths phase [11, 12, 25]. However, the observation that a localized principle eigenvector is not necessarily the fingerprint of the Griffiths phase has been reported in highly-connected networks with intrinsic weight disorder or finite-size random networks with power-law degree distributions [12, 26]. As an extension to finite dimensional models, a class of networks is found here where the Griffiths phase is absent although their principle eigenvectors are localized. As the second approach of the spectral analysis on the network connectivity matrix, the Lifschitz tails in the spectral density of the Laplacian matrix is proposed to predict the Griffiths phase analytically. Lifshitz tails have been related to the Griffiths singularity in the equilibrium systems [27]. For synchronization and spreading dynamics on networks, simulation and Quenched Mean Field approximation indicate a connection between the the Lifshitz tail and the slow dynamics [11, 28, 29]. In this study, the tail distribution of the Laplacian eigenvalues is presented to test how well it predicts the Griffiths phase in the SIS model.

This paper is organized as follows: Sec. II describes the structural properties of hierarchical modular networks,

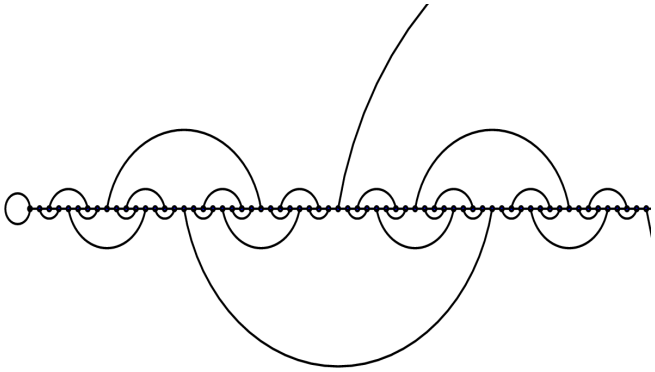

Figure 1: Depiction of the Hanoi network of generation $g = 6$. The network features a regular geometric structure, in the form of a one dimensional backbone, and a distinct set of recursive small-world links. The node degree is uniformly 3.

on which the SIS model and its critical behavior are studied; Sec.III reviews the SIS model and the spectral analysis on the adjacency matrix and the Laplacian matrix, and the analytical tools are applied to all the networks considered in this work; Sec.IV presents the numerical results for the SIS model evolving on the networks; Sec.V concludes by highlighting the significance of hierarchical level-dependent inter-module wiring probabilities on the emergence of the Griffiths phase, and discussing the essential structural characteristics for the Griffiths phase.

II. NETWORK STRUCTURE

The Hanoi networks [16, 18, 22, 23] are based on a simple geometric backbone, a one-dimensional line of $n = 2^g$ nodes. Each node is at least connected to its nearest neighbor left and right on the backbone. To construct the hierarchy to g-th generation, consider parameterizing any node $x < n$ (except for zero) *uniquely* in terms of two integers (i, j), $i \geq 1$ and $1 \leq j \leq 2^{g-i}$, via

$$x = 2^{i-1}(2j - 1). \tag{1}$$

Here, i denotes the level of hierarchy whereas j labels consecutive nodes within each hierarchy. Such a parametrization raises a natural pattern for long-range small-world edges that are formed by the neighbors $x = 2^{i-1}(4j - 3)$ and $y = 2^{i-1}(4j - 1)$ for $1 \leq j \leq 2^{g-i-1}$, as shown in Fig.(1). Eventually, this procedure constructs a finite dimensional hierarchical network with a uniform finite node degree 3, and a diameter of $\sim \sqrt{n}$, which is denoted as HN3 [16, 18, 22].

To construct a hierarchical structure that models the modular property of real-world brain networks, each single node x in HN3 is replaced by a fully-connected clique that contains a finite number m of nodes, thus forming a network with size $n \times m$. Maintaining the structural properties of HN3, the self-similar structure, and the small-world connections, I propose two connectivity patterns between modules in the same hierarchy. In the first paradigm, the single edge in the original HN3 is now formed by two randomly chosen nodes in different cliques, which I denote as HMN1. The second paradigm is inspired by previous hierarchical modular models [11, 12]. To distinguish it from HMN1, I denote it as HMN2. Previous models share common features, hierarchical construction of modules and level-dependent wiring probabilities. Modules are grouped to form larger modules in the next level. They are connected in either a stochastic way with a level-dependent probability p_i or a deterministic way with a level-dependent number of edges.

Since an infinite dimensional network is predicted not to support the Griffiths phase [11], to maintain a finite fractal dimension, the number of inter-module connections is stable across hierarchical levels. In this work, I use the stochastic scheme to construct HMN2. As the size of modules increases as level, the inter-module wiring probability decreases. In HMN2, for the first hierarchy, modules in this level are cliques themselves. Starting from the second hierarchy, the clique labeled as $2(2j-1)$ is grouped with the neighbor clique $2(2j-1)-1$ and $2(2j-1)+1$ forming a module. For the third hierarchy, the clique labeled as $2^2(2j-1)$ is grouped with three left neighbor cliques up to the clique $2^2(2j-1)-3$ and three right neighbor cliques up to the clique $2^2(2j-1)+3$. Repeating this procedure g generations, the size of module of i-th generation is $m(2^i - 1)$. The number of all possible stochastic connections between two modules is $m^2\left(4^i - 2^{i+1} + 1\right)$. Thus, to ensure at least one edge between them to exist, the level-dependent probability p_i is bounded by $1/\left(m^2\left(4^i - 2^{i+1} + 1\right)\right)$.

III. SUSCEPTIBLE-INFECTED-SUSCEPTIBLE MODEL AND THE SPECTRAL ANALYSIS

Certain fundamental dynamical models, the Susceptible-Infected-Susceptible (SIS) model and the Contact Process (CP), have been used to model the activity propagation on brain networks [11, 12]. Previous studies focus on the emergence of the Griffiths phase on general complex networks using these simplified models. Quenched disorder, either intrinsic to nodes or topological, has been shown to smear the phase transition at critical points and generate the Griffiths phase. The essential disorder may stem from a node-dependent propagation rate [30, 31]. Recent results also present evidence that the Griffiths phase emerges due to the quenched disorder on the edges, such as a correlated weight pattern in tree networks [32] and exponentially suppressed weight scheme in random networks [25].

Special *rare regions* (RRs) emerge in the dynamical process evolving on networks with quenched disorder.

Statistically, the active state lingers in these rare regions for a typical time that grows exponentially with their sizes, and eventually ends up in the absorbing state [11, 33]. Exponential size distribution of rare regions induces power-law decays with continuously varying exponents, i.e. the Griffiths phase. Not only in the spreading dynamics on networks, *rare regions* has also been shown to dramatically change the properties of classical phase transition in quenched disordered systems, such as randomly diluted Ising model or Ising model with planar defects, and quantum phase transitions in itinerant magnets with Heisenberg spin symmetry, leading to an essential singularity, the Griffiths singularity [34, 35].

In absence of the quenched disorder, the Griffiths phase can also be a consequence of the structural heterogeneity of finite dimensional networks that is expected to have a similar role as the quenched disorder [11, 30]. The Quenched Mean-Field (QMF) approximation applies a spectral analysis on the network adjacency matrix that analytically explains emerging rare regions and the Griffiths phase on networks with the quenched disorder [24, 25]. This analytical procedure successfully confirms the Griffiths phase on finite dimensional hierarchical modular networks in previous work [11]. The spectral analysis on the network Laplacian matrix provides another approach to predict the Griffiths phase, which is confirmed in [11, 29]. In this section, I will focus on the SIS model and apply the spectral analysis on all the relevant finite dimensional structures.

A. SIS Model and the Simulation

In SIS model, each node in networks is described by a binary state, active ($\sigma = 1$) or inactive ($\sigma = 0$). An active node is deactivated with a unit rate; otherwise, it propagates the active state to its inactive neighbors with a rate λ. The evolution equation for the probability $\rho_x(t)$ that node x is active at time t is

$$\frac{d}{dt}\rho_x(t) = -\rho_x(t) + \lambda\left[1-\rho_x(t)\right]\sum_{y=1}^{N} A_{xy}\rho_y(t), \quad (2)$$

in which A is the network adjacency matrix. A_{xy} is 1 if node x and y are connected by an edge; otherwise, it is 0. The Laplacian matrix of a graph is defined with the adjacency matrix as

$$L_{xy} = \delta_{xy}\sum_{z} A_{zy} - A_{xy}, \quad (3)$$

where L_{xy} is equal to $-A_{xy}$ when $x \neq y$, and L_{xx} is equal to $\sum_{y\neq x} A_{xy}$, i.e. the degree of node x. Denote eigenvalues and eigenvectors of the adjacency matrix A and the Laplacian matrix L respectively as Λ^A, $f^A\left(\Lambda^A\right)$ and Λ^L, $f^L\left(\Lambda^L\right)$.

I here briefly introduce the method used to perform the simulation for the SIS model. The large-scale numerical simulation method for the SIS model developed in [36] determines the critical propagation rate λ_c efficiently for various networks. This algorithm considers the SIS model in continuous time. At each time step, one randomly chosen active node deactives with the probability $N_i/\left(N_i+\lambda N_n\right)$ where N_i is the number of active nodes at time t, and N_n is the number of edges emanating from them. With complementary probability $\lambda N_n/\left(N_i+\lambda N_n\right)$, the active state is transmitted to one inactive neighbor of the randomly selected node. Time is incremented by $\triangle t = 1/\left(N_i+\lambda N_n\right)$. This process is iterated after updating the system.

B. The Spectral Analysis for SIS Model

In this subsection, I review the derivation of the spectral analysis on the adjacency matrix and the Laplacian matrix, and apply it to all the relevant networks. Considering the adjacency matrix, the criterion for the localization of steady active state on networks is based on the evaluation of the inverse participation ratio (IPR) of the principle eigenvector corresponding to the largest eigenvalue. Following the notations in [24], eigenvalues of the adjacency matrix are ordered as $\Lambda_1^A \geq \Lambda_2^A \geq \cdots \geq \Lambda_N^A$. The probabilities ρ_x for each node at the steady state can be written as a linear superposition of the N orthogonal eigenvectors [24],

$$\rho_x = \sum_{i=1}^{N} c\left(\Lambda_i^A\right) f_x^A\left(\Lambda_i^A\right). \quad (4)$$

If the largest eigenvalue Λ_1^A is significantly larger than all the others, the QMF approximation predicts the critical point λ_c as $1/\Lambda_1^A$, and the steady state probability as

$$\rho_x \sim c\left(\Lambda_1^A\right) f_x^A\left(\Lambda_1^A\right). \quad (5)$$

The order parameter $\rho(t)$ is defined as the average $\frac{1}{N}\sum_{x=1}^{N}\rho_x(t)$ over all the nodes. At the critical λ_c, the order parameter ρ at the steady state can be expanded as,

$$\rho \sim a_1\triangle + a_2\triangle^2 + \ldots, \quad (6)$$

in which $\triangle = \lambda\Lambda_1 - 1 \ll 1$ with the coefficients

$$a_i = \frac{\sum_{x=1}^{N} f_x^A\left(\Lambda_i^A\right)}{N\sum_{x=1}^{N}\left[f_x^A\left(\Lambda_i^A\right)\right]^3}. \quad (7)$$

With the dominant largest eigenvalue and the principle eigenvector, the order parameter ρ can be approximated with $\rho \sim a_1\triangle$. In the limit $N\to\infty$, for a localized principle eigenvector $f^A\left(\Lambda_1^A\right)$, the components $f_x^A\left(\Lambda_1^A\right)$ are of the order of $O(1)$ only at few nodes, and then $a_1 \sim O(1/N)$ and $\rho \sim O(1/N)$. Thus, the active state is localized on the a few nodes of the network. On the other hand, for a delocalized principle eigenvector $f^A\left(\Lambda_1^A\right)$, we usually have $f_x^A\left(\Lambda_1^A\right) \sim O(\frac{1}{\sqrt{N}})$, and then $a_1 \sim const$ and $\rho \sim const$. The active state extends over a finite

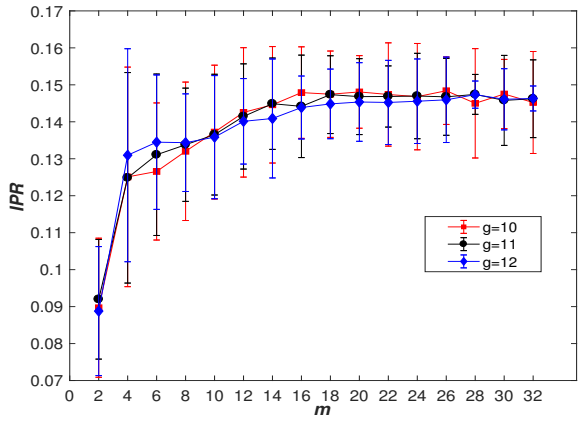

(a)

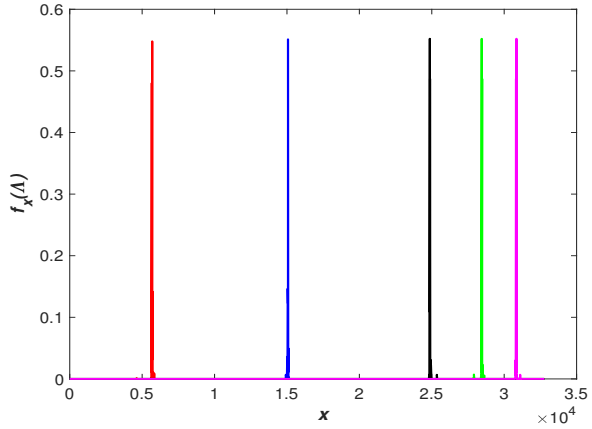

(b)

Figure 2: (a) IPR vs m for network configurations of HMN1 with different maximum generation g. The red squares are values of IPR for $g = 10$; the black circles are values of IPR for $g = 11$; the blue diamonds are values of IPR for $g = 12$. Each data point averages values of IPR over 100 independent realizations of HMN1 configuration. (b) the localized eigenvectors corresponding to five largest eigenvalues of the adjacency matrix of one graph realization of HMN1 configuration with $g = 11, m = 16$.

fraction of nodes of the network. The localization of eigenvectors is quantified by their inverse participation ratio (IPR) (shown in [24]),

$$IPR\left(\Lambda\right) = \sum_{x=1}^{N} \left[f_x\left(\Lambda\right)\right]^4. \tag{8}$$

A finite IPR value of the principle eigenvector corresponds to a localized eigenvector, while a IPR approaching to zero corresponds to a delocalized principle eigenvector. I apply the concept of IPR on all the relevant networks to examine whether a localized principle eigenvector exists, which may suggest the the emergence of rare regions and the Griffiths phase in the QMF approximation [11, 12].

As shown in Fig.(2a), the IPR of the principle eigenvector increases with clique size m towards to a finite value for different maximum generation g of HMN1. It suggests the principle eigenvectors for HMN1 configurations are localized. Additionally, localized eigenvectors corresponding to largest eigenvalues are also found, shown in Fig.(2b). For HMN2, I focus on level-dependent inter-module wiring probabilities, $p_i = 4^{-(i+1)}$ and $p_i = 4^{-i}$ in this work. The backbone as well as the first level inter-module wiring probability is fixed at 1/4, where the modules are the basic cliques described in Sec.II. Values of IPR are shown in Fig.(3a). The largest value comes from the network configuration that the single clique contains 2 nodes, and the probability is $p_i = 4^{-(i+1)}$. In this case, the network is statistically almost fragmented. Numerical results in Sec.IV indeed show the emergence of the Griffiths phase as a trivial consequence of the network disconnectedness. To examine the Griffiths phase on a connected network with a finite fractal dimension, the network configuration of $m = 3$ and $p_i = 4^{-(i+1)}$ is also chosen for the numerical simulation. For stochastically constructed HMN2, as the clique size m or level-dependent probability increases while keeping the other factor fixed, modules becomes more and more connected with other modules in the same level, and the value of IPR decreases, shown in Fig.(3a). The regime over the parameter m and the level-dependent p_i that possibly supports the Griffiths phase is narrow. It is not surprising to see that the localized principle eigenvector exists for network configurations of HMN2 with a finite value of IPR. In Fig.(3b) and Fig.(3c), I illustrate the localized eigenvectors corresponding to large eigenvalues in two network configurations.

As a second approach of the spectral analysis to further confirm the Griffiths phase, I study the spectral density of the network Laplacian at the lower edge, the Lifshitz tail. The Laplacian matrix is positive semidefinite, i.e. $\Lambda_i^L \geq 0$ and $\Lambda_1^L = 0$, following the notations in [29]. The smallest nonzero Λ_2^L is defined as the spectral gap. Near the critical point, in the inactive phase, the evolution equation of the SIS model Eq.(2) can be approximated as

$$\frac{d}{dt}\rho_x\left(t\right) = -\rho_x\left(t\right) + \lambda \sum_{y=1}^{N} A_{xy}\rho_y\left(t\right), \tag{9}$$

which can be rewritten using the Laplacian matrix as

$$\frac{d}{dt}\rho_x\left(t\right) = \left(\lambda\delta_{xy}\sum_{z=1}^{N} A_{yz} - 1\right)\rho_x\left(t\right) - \lambda\sum_{y=1}^{N} L_{xy}\rho_y\left(t\right). \tag{10}$$

A linear stability analysis is performed [29], similar to the synchronization process [37]. The normal modes of the

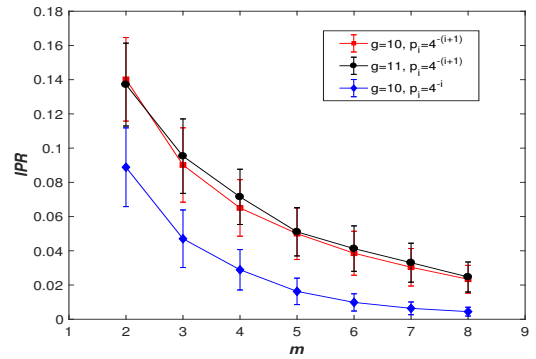

(a)

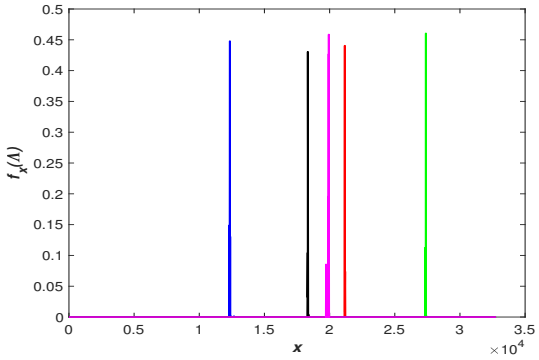

(b)

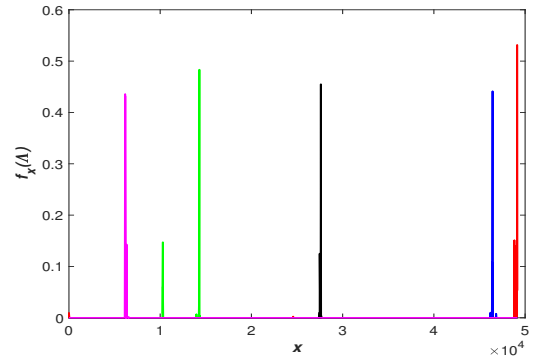

(c)

Figure 3: (a) IPR vs m for network configurations of HMN2 with different g. The red squares are values of the IPR with $g = 10$; the black circles are IPRs for $g = 11$. The hierarchical level-dependent inter-module probability is $p_i = 4^{-(i+1)}$. Compared to them, the blue diamonds are IPRs for $g = 10$ with a level-dependent probability $p_i = 4^{-i}$. Each data point averages IPRs over 100 independent realizations of HMN2 configuration. (b): localized eigenvectors corresponding to five largest eigenvalues of the adjacency matrix of one graph realization of HMN2 configuration with $g = 14, m = 2, p_i = 4^{-(i+1)}$; (c): localized eigenvectors corresponding to five largest eigenvalues of the adjacency matrix of one graph realization of HMN2 with $g = 14, m = 3, p_i = 4^{-(i+1)}$.

perturbations above the absorbing state can be written,

$$\frac{d}{dt}\rho_x(t) = -\lambda \sum_y L_{xy}\rho_y(t). \tag{11}$$

Using the Laplacian spectrum, $\rho_x(t)$ can be expressed as the expansion with the Laplacian eigenvalues and eigenvectors,

$$\rho_x(t) = \sum_{iy} e^{-\lambda\Lambda_i^L t} f_x^L\left(\Lambda_i^L\right) f_y^L\left(\Lambda_i^L\right) \rho_y(0), \tag{12}$$

and the total density is determined by the lowest eigenvalues of the spectrum,

$$\rho(t) \sim \sum_{i=2}^{N} e^{-\lambda\Lambda_i^L t}. \tag{13}$$

In the continuum limit,

$$\rho(t) \sim \int_{\Lambda_2^L}^{\Lambda_c^L} d\Lambda P(\Lambda) e^{-\lambda\Lambda t}, \tag{14}$$

in which Λ_c^L is the experimentally determined end of tail value. A power-law distribution $P(\Lambda)$ of the lower edge of the Laplacian spectrum suggests the Griffiths phase behavior above the absorbing state [29].

$$\rho(t) \sim \int_{\Lambda_2}^{\Lambda_c} d\Lambda\Lambda^a e^{-\lambda\Lambda t}, \tag{15}$$

$$\sim t^{-\lambda(a+1)}, \tag{16}$$

For comparison I calculated the Lifshitz tails for HMN1 and HMN2, shown in Fig.(4). In the plot, the probability distribution $P(\Lambda)$ is calculated with the bin size $\delta\Lambda = 0.0001$ over 100 independent graph realizations. The Lifshitz tail for HMN2 configuration with $g = 13, m = 2, p_i = 4^{-(i+1)}$, and with $g = 12, m = 3, p_i = 4^{-(i+1)}$, are fitted with power laws as,

$$P(\Lambda) \sim \Lambda^{0.6828\cdots}, \tag{17}$$

and

$$P(\Lambda) \sim \Lambda^{0.8226\cdots}, \tag{18}$$

while the Lifshitz tail for HMN1 slightly deviates from a power law, suggesting the lack of the Griffiths phase according to [29].

IV. SIMULATION RESULTS FOR THE SIS MODEL ON HMN1 AND HMN2

In this section, I present results from numerical study of the SIS model on all the network configurations of HMN1 and HMN2 using the simulation method introduced in Sec.III A. The network is initialized as a fully-active graph. The system is updated each step until the maximum time t_{max} $\left(10^6\right)$ is reached or in case of activity extinction. Simulations for each propagation rate λ

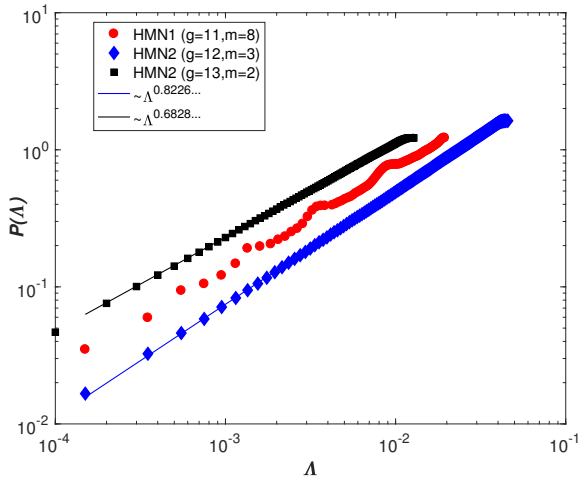

Figure 4: Lifshitz tails for HMN1 and HMN2: The red circles are tail distribution for HMN1 configuration with $g = 11, m = 8$; the black squares are tail distribution for HMN2 configuration with $g = 13, m = 2, p_i = 4^{-(i+1)}$, fitted with a power law $P(\Lambda) \sim \Lambda^{0.6828\cdots}$; the blue diamonds are tail distribution for HMN2 configuration with $g = 12, m = 3, p_i = 4^{-(i+1)}$, fitted with $P(\Lambda) \sim \Lambda^{0.8226\cdots}$.

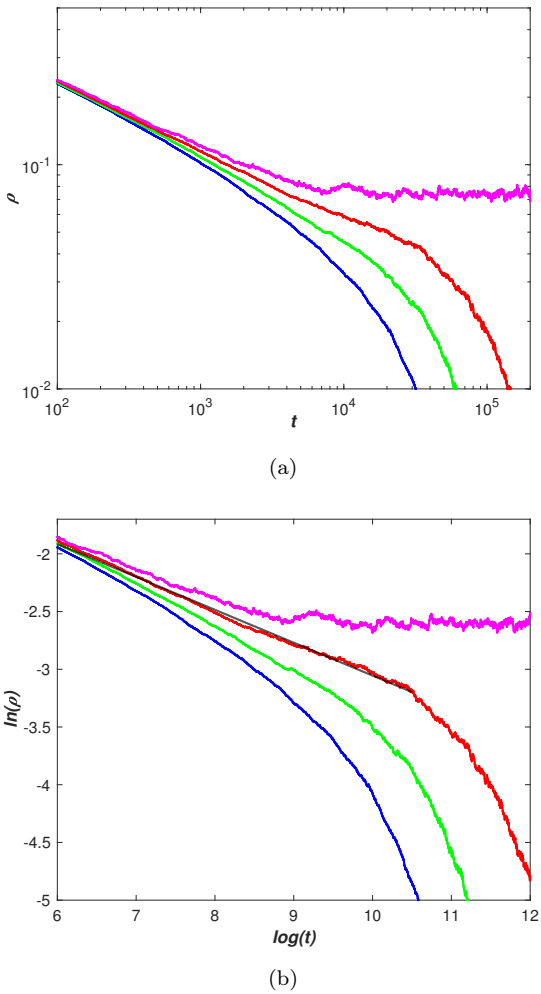

Figure 5: (a): ρ vs t for network configuration of HMN1 with $g = 11, m = 8$. Lines from bottom to top are for $\lambda = 0.1650, 0.1651, 0.1652, 0.1653$. (b): $\log(\rho)$ versus $\log(t)$, the black straight line is the fitted curve with $\rho \sim t^{-0.2849\cdots}$. The critical propagation rate is $\lambda_c \approx 0.1652$

are repeated on $1000 \sim 5000$ independent network realizations. The order parameter $\rho(t)$ for each λ is the average of all the runs. I also derive the effective decay exponent by fitting critical power laws $\rho(t) \sim t^{-\alpha_{eff}}$ with the efficient exponent defined as ([12, 25])

$$\alpha_{eff} = -\frac{\ln[\rho(t)/\rho(t')]}{\ln(t/t')}. \tag{19}$$

Fig.(5) and Fig.(6) present the simulation results for network configurations of HMN1 with $g = 11, m = 8$ and $g = 11, m = 16$, and fit with the effective decay exponent at the critical point. It shows that the Griffiths phase is absent in HMN1, and we see a trivial phase transition at a single critical point. For network configuration of HMN2 with $m = 2$ and $p_i = 4^{-(i+1)}$, the size-independent Griffiths phase emerges, shown in Fig.(7). However, the Griffiths phase is a trivial consequence of the disconnectedness of HMN2 as discussed in Sec.III B. For network configurations of HMN2 that is connected, I choose the case of $m = 3, p_i = 4^{-(i+1)}$ at which the corresponding value of IPR is sufficiently large. Since inter-module connections are established stochastically, there is a chance that all the possible inter-module edges fails to be connected. To avoid this case, at least one inter-module connection is enforced to exist by repeating the construction of graphs in the simulation. Numerical results for a connected HMN2 is presented in Fig.(8). We see a nearly size-independent power laws in a stretched regime of λ. Comparing Fig.(7) with Fig.(8), as m increases while keeping p_i fixed and *vice versa*, the regime in the parameter space of λ for the Griffiths phase is expected to become narrow until it disappears when HMN2 becomes highly connected.

As introduced in Sec.I, one significant advantage of biological systems operating at criticality is the diverging reaction to highly diverse stimuli. From the perspective of statistical mechanics, this is caused by the divergence of susceptibility at criticality. To measure the divergence of response in the Griffiths phase, here I use the concept of dynamic susceptibility that is applied to gauge the overall response to a continuous localized stimulus in [11]. This dynamic susceptibility is defined as,

$$\Sigma(\lambda) = N[\rho_f(\lambda) - \rho_s(\lambda)], \tag{20}$$

where $\rho_s(\lambda)$ is the stationary density in the absence of stimuli and $\rho_f(\lambda)$ is the steady-state density reached

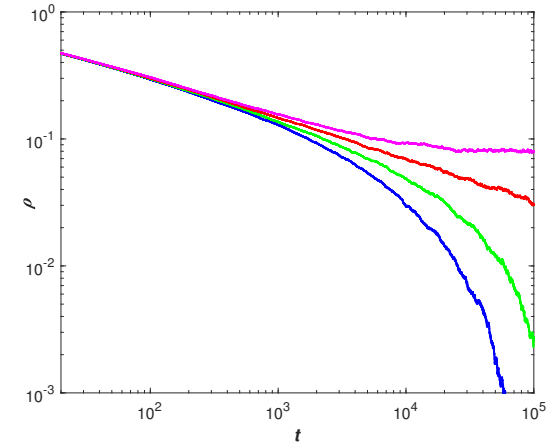

(a)

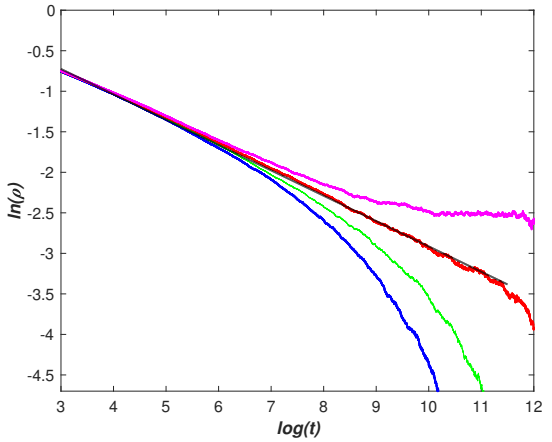

(b)

Figure 6: (a): ρ vs t for network configuration of HMN1 with $g = 11, m = 16$. Lines from bottom to top are for $\lambda = 0.07475, 0.07480, 0.07485, 0.0749$. (b): $\log(\rho)$ versus $\log(t)$, the black straight line is the fitted curve with $\rho \sim t^{-0.3127\cdots}$. The critical propagation rate is $\lambda_c \approx 0.07485$.

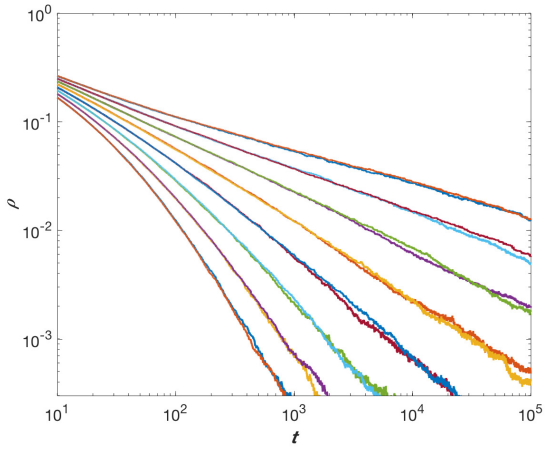

(a)

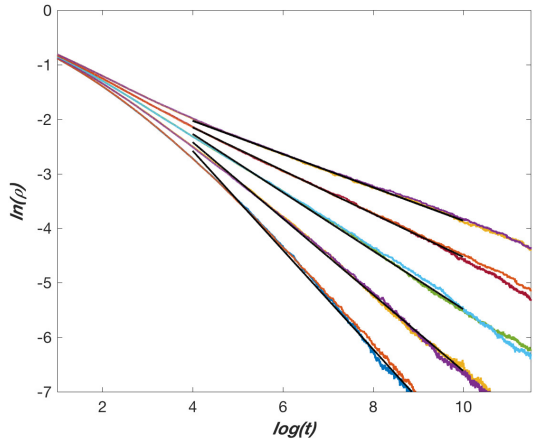

(b)

Figure 7: (a): ρ vs t for network configurations of HMN2 with $g = 13, m = 2$ and with $g = 14, m = 2$. Lines from bottom to top are for $\lambda = 0.46, 0.47, 0.48, 0.49, 0.50, 0.51, 0.52, 0.53$. (b): $\log(\rho)$ versus $\log(t)$, the black straight lines are the fitted curves with $\rho \sim t^{-0.9094\cdots}$, $\rho \sim t^{-0.6989\cdots}$, $\rho \sim t^{-0.5356\cdots}$, $\rho \sim t^{-0.3962\cdots}$ and $\rho \sim t^{-0.3054\cdots}$ from bottom to top for $\lambda = 0.49, 0.50, 0.51, 0.52, 0.53$

when one single node is constrained to remain active. As shown in Fig.(9), Σ becomes large in the region of the Griffiths phase, and more importantly it grows with the network size N that implies a divergent response over an extended region.

V. CONCLUSION

The Griffiths phase induced purely by the structural disorder suggests an alternative self-organizing mechanism for brain function. Brain networks are shown to have strong modularity, and densely connected modules are organized in a hierarchical pattern. Another important feature found empirically is the small-world topology that ensures the efficient information transfer between modules. To solve the the conundrum between small-world topology and large-world architecture of brain networks, incorporating progressively weaker inter-module connections while maintaining well defined modules is proposed as a solution [38]. In this work, I construct two classes of synthetic hierarchical modular networks that incorporate weak inter-module connections in distinguished ways. The first model HMN1 builds the hierarchical small-world connections into the planar modular networks. The second model HMN2 organizes modules into hierarchies, and the inter-module wiring probability is level-dependent. Both of them possess a self-similar structure and small-world long range connections, based on the 3-regular Hanoi network [23].

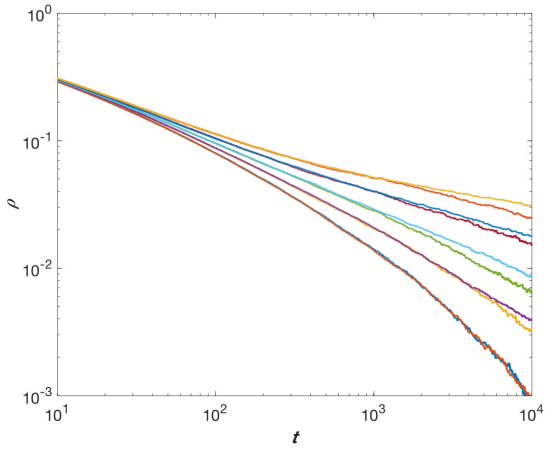

(a)

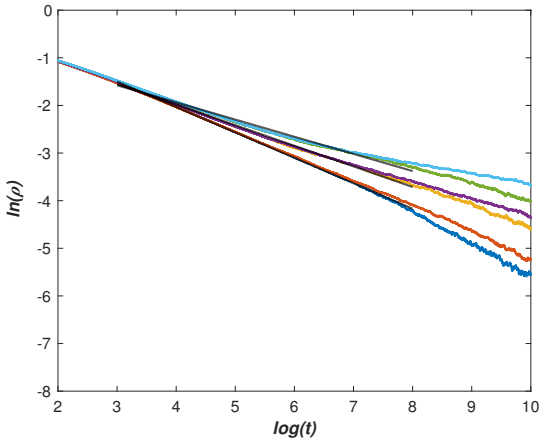

(b)

Figure 8: (a): ρ vs t for network configurations of HMN2 with $g = 13, m = 3$ and with $g = 12, m = 3$. Lines from bottom to top are for propagation rates $\lambda = 0.258, 0.259, 0.260, 0.261, 0.262$. (b): $\log(\rho)$ versus $\log(t)$, the black straight lines from bottom to top are the fitted curves with $\rho \sim t^{-0.5339\ldots}$, $\rho \sim t^{-0.4325\ldots}$, $\rho \sim t^{-0.3605\ldots}$ for $\lambda = 0.260, 0.261, 0.262$

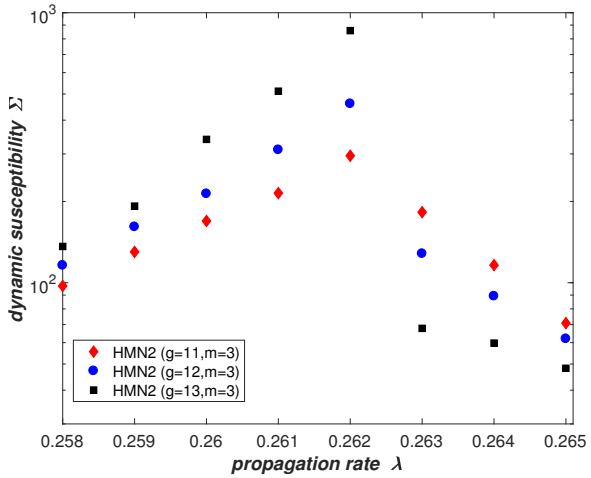

Figure 9: : Dynamic susceptibility Σ, measured for network configurations of HMN2 with $g = 11, m = 3$ (red diamonds), $g = 12, m = 3$ (blue circles) and $g = 13, m = 3$ (black squares) with the $p_i = 4^{-(i+1)}$. The overall response increases significantly near and in the Griffiths phase (from $\lambda = 0.260$ to $\lambda = 0.262$), and decreases away from the critical region.

I study the Griffiths phase by evolving the fundamental SIS model on the HMNs designed. As an further exploration into the Griffiths phase caused by the structural heterogeneity of networks, I present numerical results for two classes of networks. The results suggest the essential role of level dependent inter-module wiring probability on the emergence of the Griffiths phase. The first class of hierarchical networks, HMN1, are not able to support the Griffiths phase, although they satisfy the structural criteria, such as the finite fractal dimension, the modular structure, the hierarchical heterogeneity. The second class of hierarchical networks, HMN2, are constructed to possess a hierarchical pattern in the inter-module wiring probabilities, which therefore require a delicate tuning to maintain a connected, finite dimensional network. The hierarchical pattern of inter-module connections results in more heterogeneous networks of HMN2, while network configurations of HMN1 are more homogenous. This can be shown by considering the Lifshitz tails for HMN1 and HMN2 in Fig.(4). The Lifshitz tail of HMN1 deviates from that of HMN2, and compared to HMn2, the spectrum of HMN1 is closer to the original network HN3 [39]. Although HN3 possesses a hierarchical structure, it is not sufficiently disordered to induce the Griffiths phase. The difference between hierarchical patterns of HMN1 and HMN2 significantly affects the phase transition and existence of the Griffiths phase.

As a complement to the computational efforts, the spectral analysis proposed in the Quenched Mean Field approximation suggests that a finite IPR of the principle eigenvector of the adjacency matrix can be considered to indicate the localization of activity that may result in the emergence of rare regions and the Griffiths phase under certain circumstances. Although all the network configurations of HMN1 prove to have a finite IPR and localized eigenvectors corresponding to the largest eigenvalues, only when the structural disorder of inter-module connections is sufficient as in HMN2, the Griffiths phase appears. As a counter example to previous finite dimensional models with localized principle eigenvectors that support the Griffiths phase [11, 12], a class of finite dimensional networks with a localized principle eigenvector is found where the Griffiths phase is absent. This raises questions on a more generalized theoretical analysis on the network adjacency matrix that applies to all the networks considered previously and currently. Besides the spectral analysis on the adjacency matrix, the Lifshitz

tail of Laplacian spectrum presents a power law probability distribution at the lower edge of spectrum of HMN2 networks, while the tail distribution in HMN1 deviates from a power law. Numerical results confirm the property of phase transition may be related to this difference between Lifshitz tails of HMN1 and HMN2.

VI. ACKNOWLEDGEMENTS

I would like to thank Prof. Stefan Boettcher for helpful discussions. This work is supported by the NSF through grant DMR-1207431 is gratefully acknowledged.

[1] M. Nykter, N. D. Price, M. Aldana, S. A. Ramsey, S. A. Kauffman, L. E. Hood, O. Yli-Harja, and I. Shmulevich, Proceedings of the National Academy of Sciences **105**, 1897 (2008).
[2] C. Furusawa and K. Kaneko, Phys. Rev. Lett. **108**, 208103 (2012), URL `http://link.aps.org/doi/10.1103/PhysRevLett.108.208103`.
[3] J. M. Beggs and D. Plenz, The Journal of neuroscience **23**, 11167 (2003).
[4] D. Plenz and T. C. Thiagarajan, Trends in neurosciences **30**, 101 (2007).
[5] J. M. Beggs, Philosophical Transactions of the Royal Society of London A: Mathematical, Physical and Engineering Sciences **366**, 329 (2008).
[6] O. Kinouchi and M. Copelli, Nature physics **2**, 348 (2006).
[7] R. Legenstein and W. Maass, Neural Networks **20**, 323 (2007).
[8] R. Barbieri and M. Shimono, Networking of Psychophysics, Psychology and Neurophysiology p. 61 (2012).
[9] M. Rubinov, O. Sporns, J.-P. Thivierge, and M. Breakspear, PLoS Comput Biol **7**, e1002038 (2011).
[10] S.-J. Wang and C. Zhou, New Journal of Physics **14**, 023005 (2012).
[11] P. Moretti and M. A. Muñoz, Nature communications **4** (2013).
[12] G. Ódor, R. Dickman, and G. Ódor, Scientific reports **5** (2015).
[13] O. Sporns, D. R. Chialvo, M. Kaiser, and C. C. Hilgetag, Trends in cognitive sciences **8**, 418 (2004).
[14] D. Meunier, R. Lambiotte, and E. T. Bullmore, Frontiers in neuroscience **4**, 200 (2010).
[15] M. Kaiser, Neuroimage **57**, 892 (2011).
[16] S. Boettcher, J. L. Cook, and R. M. Ziff, Physical Review E **80**, 041115 (2009).
[17] A. N. Berker, M. Hinczewski, and R. R. Netz, Physical Review E **80**, 041118 (2009).
[18] S. Boettcher and C. T. Brunson, Phys. Rev. E **83**, 021103 (2011).
[19] S. Boettcher, V. Singh, and R. M. Ziff, Nature communications **3**, 787 (2012).
[20] V. Singh and S. Boettcher, Physical Review E **90**, 012117 (2014).
[21] V. Singh, C. T. Brunson, and S. Boettcher, Phys. Rev. E **90**, 052119 (2014).
[22] S. Boettcher, B. Gonçalves, and H. Guclu, Journal of Physics A: Mathematical and Theoretical **41**, 252001 (2008).
[23] S. Boettcher and S. Li, Journal of Physics A: Mathematical and Theoretical **48**, 415001 (2015).
[24] A. V. Goltsev, S. N. Dorogovtsev, J. G. Oliveira, and J. F. F. Mendes, Phys. Rev. Lett. **109**, 128702 (2012).
[25] G. Ódor, Physical Review E **88**, 032109 (2013).
[26] W. Cota, S. C. Ferreira, and G. Ódor, Phys. Rev. E **93**, 032322 (2016).
[27] T. M. Nieuwenhuizen, Phys. Rev. Lett. **63**, 1760 (1989).
[28] P. Villegas, P. Moretti, and M. A. Muñoz, Scientific reports **4** (2014).
[29] G. Ódor, Phys. Rev. E **90**, 032110 (2014).
[30] M. A. Muñoz, R. Juhász, C. Castellano, and G. Ódor, Physical review letters **105**, 128701 (2010).
[31] R. Juhász, G. Ódor, C. Castellano, and M. A. Muñoz, Physical Review E **85**, 066125 (2012).
[32] G. Odor and R. Pastor-Satorras, Physical Review E **86**, 026117 (2012).
[33] R. B. Griffiths, Physical Review Letters **23**, 17 (1969).
[34] T. Vojta, Journal of Physics A: Mathematical and General **39**, R143 (2006).
[35] T. Vojta and J. Schmalian, Physical Review B **72**, 045438 (2005).
[36] S. C. Ferreira, C. Castellano, and R. Pastor-Satorras, Physical Review E **86**, 041125 (2012).
[37] M. Barahona and L. M. Pecora, Phys. Rev. Lett. **89**, 054101 (2002).
[38] L. K. Gallos, H. A. Makse, and M. Sigman, Proceedings of the National Academy of Sciences **109**, 2825 (2012).
[39] S. Boettcher and S. Li, arXiv preprint arXiv:1607.05168 (2016).